Utilizing the deuterium-tritium fusion resonance to diagnose thermal runaway in igniting plasmas

Robert H. Dwyer,[1,2,3,*] K. D. Meaney,[1] B. M. Haines,[1] B. J. Albright,[1] H. Geppert-Kleinrath,[1] J. P. Sauppe,[1] W. Daughton,[1] N. M. Hoffman,[1] C. Forrest,[3] S. P. Regan,[3] and Y. Kim[1]

[1]*Los Alamos National Laboratory, Los Alamos, New Mexico 87545, USA*

[2]*Laboratory for Laser Energetics, University of Rochester, Rochester, New York 14623, USA*

[3]*Department of Mechanical Engineering, University of Rochester, Rochester, New York 14611, USA*

(Received 20 May 2025; accepted 27 February 2026; published 27 March 2026)

For high-efficiency inertial confinement fusion implosions, it is predicted that a burning hot spot will successfully encompass all surrounding fuel and then transition into a thermal runaway where the internal energy increase from fusion occurs on a timescale faster than the expansion of the fuel is able to quench the fusion chain reaction after ignition occurs. Observation of this dynamic phase transition would indicate distinct burn properties and indicate an implosion's robustness. A technique for diagnosing the presence of thermal runaway from measurements of nuclear reaction history is presented. The technique is based on taking the logarithmic derivative of the nuclear reaction history, called the α curve, and allowing a mathematical decoupling of the mass, volume, and thermal reactivity in the fusion reaction rate equation. During thermal runaway, where the thermal temperature dominates the burn dynamics, a maximum in the α curve is found where there is a maximum in the first derivative of the thermal fusion reactivity, an effect to the deuterium-tritium (DT) fusion cross-section resonance. This provides a distinct signature related to the fundamental nature of the DT fusion nuclear resonance and signifies the transition into the fusion thermal instability. Impacts of charged particle transport on the effect are also assessed and the analytical formulas are compared and found to be in agreement with radiation hydrodynamic codes.

DOI: 10.1103/pl89-ftjd

I. INTRODUCTION

Inertial confinement fusion (ICF) seeks to generate more fusion energy from nuclear fusion reactions than the energy required to heat and compress the fuel to fusion conditions. The condition to generate more fusion energy from fusion than the compression work typically requires an areal density greater than 0.4 g/cm^2 and temperatures greater than 4.5 keV [1–3]. This requires high implosion velocities, typically greater than 300 km/s [4]. The National Ignition Facility (NIF) achieves these conditions by placing a fuel capsule in the center of a cylindrical high-Z cavity (hohlraum), which is illuminated by 1.8–2.2 MJ of UV light. The laser light is converted to x rays by the hohlraum, which then ablate the outer layer of the fuel capsule, causing the fuel to implode [5–7].

The only design that has demonstrated success for high-gain ICF implosions is the hot-spot ignition design, where the fuel capsule consists of a low-density deuterium-tritium (DT) vapor in the center, surrounded by high-density DT ice. The ice is surrounded by a high-density carbon (HDC) ablator which generates the pressures to drive the implosion from the x rays [8]. The ice acts as a pusher that implodes the fuel and heats it to the necessary conditions to produce thermonuclear fusion reactions, forming a "hot spot." Once this hot spot ignites and generates more fusion energy than is coupled to the fuel from the compressive work, the ignited hot spot then drives a burn wave into the DT ice, increasing the fuel mass participating in thermonuclear burn and therefore energy gain. Since December 2022 NIF has successfully ignited multiple experiments that produce more total fusion energy than the driver laser coupled to the capsule [9–11].

Previous theoretical work and simulations have concluded that the burn propagation is primarily driven by ablation of the ice mass into the hot spot [12,13]. Before the hot spot ignites, the mass ablation is primarily driven by electron thermal conduction from the hot spot into the ice [14–17]. Recent work has shown that in the ignition regime the α-particle, x-ray, and neutron flux driven into the ice by the burning hot spot will significantly enhance the mass ablation into the hot spot, driving the propagating ablative burn wave.

During the burn-propagation phase of the implosion the rapid increase in mass will increase the reaction rate but tamp the temperature growth rate of the hot spot due to the rapidly increasing hot-spot energy from fusion distributing itself over the hot-spot mass. Once the burn propagation is finished and the hot spot has grown to contain all the ice mass, then the fuel mass is fixed and the temperature of the hot spot will enter the thermal runaway phase where the hot spot rapidly increases in temperature, further increasing the fusion rate. The thermal

*Contact author: rdwyer@lanl.gov

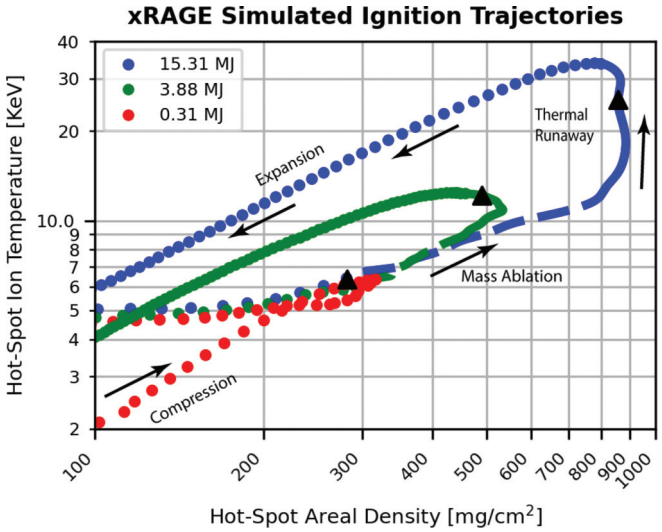

FIG. 1. XRAGE simulations showing a burning plasma (red), a marginally igniting plasma (green), and a robustly ignited plasma that initiates thermal runaway (blue). The colored dots denote the compression-dominated regions, the dashed lines denote the mass ablation phase of the implosion, and the solid line is the temperature-dominated phase. The "x" indicates the nuclear bang time of the implosion where the fusion yield rate, dY/dt, is at its maximum.

runaway phase is characterized by the growth in temperature occurring on a timescale faster than the decompression of the hot spot such that $dT/d\rho R \to \infty$. This process then is only stopped by the expansion or burnup of the fusion fuel, which begins the decompression phase of the implosion.

Entering the thermal runaway phase is advantageous to the ICF experiment as rapidly increasing temperature increases the specific hot-spot energy $e_{hs} = E_{hs}/m_f$, where m_f is the fuel mass and E_{hs} is the total hot-spot energy. This will increase the robustness of the fusion burn to yield degradation mechanisms such as mixing of cold high-Z reactants into the hot spot. The rapid increase in temperature also means that more expansion is required to quench the fusion burn and therefore it will increase the burnup fraction.

Hydrodynamic simulations suggest that this transition into thermal runaway will occur with NIF yields around 8 MJ, slightly higher than the currently achieved 5.2 MJ [18,19]. Simulations have predicted that this transition is characterized by ignition occurring before peak compression, while the capsule is still imploding and during nuclear bang time, where the yield rate, dY/dt, is at its maximum, occurs at peak compression rather than during the expansion of the fuel. Figure 1 shows example ignition trajectories of nonigniting, marginally igniting, and robustly igniting implosions where the thermonuclear runaway is initiated [19].

Since fusion yield scales with both ion temperature and fuel mass, an observed increase in the total yield or gain of the target does not necessarily imply a thermal instability has been created. Ion temperature measurements are likewise burn averaged over both the temperature rise and the fast expansion. Furthermore, due to the fast expansion rate of the fuel, the fast flow speeds additionally broaden the neutron pulse width, complicating ion temperature measurements from neutron time-of-flight (nTOF) diagnostics [20–23]. Calculations of this effect have indicated that the measured ion temperature from the spectral width differs significantly from the true burn-averaged temperature [22,24]. Simulations predict that short burn widths (<50 ps) and high downscatter ratio (>4%) are potentially indicative of thermal runaway; however, the exact trend is dependent on the mode of yield degradation such as the mechanisms of mixing, shell defects, and preheat [19]. Currently, no time-resolved ion temperature or areal density diagnostics exist to reproduce an experimental curve such as the one in Fig. 1. Therefore, a dynamic signature that can diagnose the seeding of thermal runaway is desirable [25].

The transition from burn propagation to the initiation of thermal runaway to heat the fuel is a rapid and dynamic process and therefore requires a dynamic measurement to accurately diagnose. This work investigates signatures unique to thermal runaway that would be present in measurements of the nuclear reaction history. Nuclear reaction history is a measurement of the nuclear reaction rate as a function of time and provides the nuclear bang-time and burn-width measurements of the implosions of the NIF. It is the only diagnostic technique that can measure the dynamics of thermonuclear burn [26–28]. The logarithmic derivative (α curve) of the reaction history was found to have a unique signature that indicates the presence of thermal runaway where the α curve spikes and has a maximum at an ion temperature of approximately 14.4 keV for DT fusion. This is due to the resonance in the DT cross section impacting the thermal reactivity $\langle \sigma v \rangle$. The impact of charged particle transport was found to lower this temperature for low areal densities (see Appendix B) but is within the uncertainty of the fits to the cross section at NIF ignition-shot-relevant areal densities.

This condition provides a distinct signature of thermal runaway in fusion plasmas, which enables the measurement of the change from marginal to robust ignition in ICF implosions to be measured. While the focus of this paper is on current NIF-scale experiments, this condition will be common to all platforms that seek to seed a thermal instability to generate high gain from fusion self-heating, including direct-drive experiments, pulsed-power-driven systems, and next-generation ICF experiments.

II. MAXIMUM OF THE α CURVE IN THERMAL RUNAWAY

Derivation of $\alpha_{\max}$ in thermal runaway

The goal of thermonuclear fusion is to generate α-particle self-heating of the fusion fuel, which will further drive more fusion reactions. However, in ICF, the heat losses in the hot spot must be overcome, such as radiation losses, thermal conductivity energy losses, and expansion work on the pusher done by the fuel. This leads to a power-balance equation [12,17,29–31]:

$$\frac{dE}{dt} = q_\alpha + q_{PdV} - q_\gamma - q_e + q_M. \tag{1}$$

Here $\frac{dE}{dt}$ is the total power of the hot spot, q_α is the α-particle heating rate in the hot spot, q_{PdV} is the gain or loss in energy due to the compressive work done on the fuel, q_γ is the radiation loss, q_e is the thermal conductivity loss, and q_M is the

change in energy due to the enthalpy flux from the ablating ice mass into the fuel, defined as $q_M = h\frac{dM}{dt}$ [12]. Neutron heating in the hot spot is generally considered negligible; however, recent work has demonstrated that it is important for understanding the ablation rate of the ice into the hot spot during the burn-propagation phase [12].

After ignition, if the q_α term is much larger than the rest of the gains or losses, the rest of the power-balance terms can be ignored, which leads to the equation of thermal runaway,

$$\frac{dE}{dt} = q_\alpha \rightarrow m_f c_v \frac{dT}{dt} = f_\alpha Q_{\text{fus}} \frac{dY}{dt}. \tag{2}$$

Here, Q_{fus} is the fusion energy released in the α particle, f_α is the fractional energy deposition of the α particle in the fuel, m_f is the fusion fuel mass in the hot spot, and c_v is the specific heat capacity. In this thermal runaway regime, the burnup rate is not yet high enough to decrease the reaction rate, and the fusion heating outpaces the expansion. The thermal runaway regime is stopped either by the burnup of the fuel or the rapid expansion quenching the reaction rate and temperature, invalidating Eq. (2).

The reaction rate $\frac{dY}{dt}$ is the number of fusion reactions per second within the volume of the fuel, given by as

$$\frac{dY}{dt} = g_\alpha n_{\text{D}} n_{\text{T}} \langle \sigma v(T) \rangle V. \tag{3}$$

Here, n_{D} and n_{T} are the particle number densities of the deuterium and tritium, respectively; V is the fuel volume; and $\langle \sigma v(T) \rangle$ is the thermal reactivity, which is a function of the fuel temperature (T) for a Maxwellian plasma [32,33]. g_α is a constant for the correction of the burn-volume-averaged yield rate from an isobaric hot-spot profile [34]. Writing Eq. (3) in terms of the total number density of the fuel leads to

$$\frac{dY}{dt} = x(1-x) g_\alpha n_f^2 \langle \sigma v(T) \rangle V, \tag{4}$$

where x is the fraction of deuterium in the total fuel mass [$x \equiv n_{\text{D}}/(n_{\text{D}} + n_{\text{T}})$].

In ICF, once the central hot spot ignites, the rapid ablation of ice into the hot spot increases the fuel mass. This increase in mass is independent of the compression of the hot spot by the ice and will still occur even if the pusher is stagnant. Therefore, Eq. (4) is modified to include the fuel mass term rather than the density term; using $\rho = m_f/V$ and $n_f = m_f N_a / A_{\text{DT}}$ yields

$$\frac{dY}{dt} = \frac{x(1-x) g_\alpha N_a^2 m_f^2 \langle \sigma v(T) \rangle}{A_{\text{DT}}^2 V}, \tag{5}$$

where N_a is Avogadro's number and A_{DT} is the average atomic number of the deuterium and tritium atoms.

In ICF experiments, $\frac{dY}{dt}(t)$ is measured utilizing gas Cherenkov detectors which measure the 16.7-MeV DT fusion γ ray from the D(T, γ)^{5}He reaction. In recent years, rapid advances in Cherenkov detector technology, such as the addition of pulse dilation photomultiplier tubes, have enabled temporal resolution measurements of less than 10 ps to be taken on the NIF [35,36]. This resolution is fast enough to capture the fast dynamics of the ignited plasma and enables the logarithmic derivative of the reaction rate to be accurately taken, which is the relative derivative of the reaction rate, or "α curve" ($\alpha(t) = \frac{d}{dt} \ln \frac{dY}{dt}$) which, for time-changing mass, temperature, and volume, gives [37]

$$\alpha(t) = \frac{2}{m_f}\frac{dm_f}{dt} + \frac{1}{\langle \sigma v(T) \rangle}\frac{d\langle \sigma v(T) \rangle}{dt} - \frac{1}{V}\frac{dV}{dt}. \tag{6}$$

The advantage of Eq. (6) for analyzing measurements of the reaction history is clear due to the relative derivatives of the mass, volume, and reactivity terms being added rather than multiplied and that the constants are eliminated in the reaction rate equation. Therefore, if one of the terms dominates the reaction rate, the others can be ignored.

The relationship between the fusion yield rate in Eq. (5) and the internal energy in Eq. (2) leads to a nonlinear function and a rapid growth rate in temperature as the fusion thermal reactivity is a function of temperature. Often simple analytical assumptions are made such as $\langle \sigma v \rangle \approx a T^b$, which for $b = 1$ would lead to a first-order nonlinear differential equation when substituted into Eqs. (5) and (2), which leads to an exponential increase in the temperature. For the temperature regime of igniting plasmas (8–25 keV), $b = 2$ is typically used [3,14,38,39] and an asymptotically increasing solution is found. These simplified relations, while too simple to fully describe the dynamic processes in thermonuclear burning plasmas, demonstrate the speed at which thermal runaway increases the hot-spot internal energy.

In a plasma that achieves thermal runaway, these simple relations demonstrate that the energy losses such as from expansion or mixing during the burn must decrease the internal energy at a faster-than-exponential rate to quench the fusion burn and prevent temperature growth, making the burn more robust to typical energy degradation mechanisms. Thus, it is a reasonable approximation that, in the early phase of thermal runaway, after the burn-propagation phase of the implosion is finished, the mass and volume terms in Eq. (6) can be dropped as the increase in temperature is faster than the initial hydrodynamic expansion of the fuel. After applying the chain rule to separate the reactivity's dependence on temperature and time, the following equation is found:

$$\alpha(t) \approx \frac{1}{\langle \sigma v(T) \rangle}\frac{d\langle \sigma v(T) \rangle}{dt} = \frac{1}{\langle \sigma v(T) \rangle}\frac{d\langle \sigma v(T) \rangle}{dT}\frac{dT}{dt}. \tag{7}$$

Substituting Eq. (2) into Eq. (7), assuming $f_\alpha \approx 1$, then yields

$$\alpha(t) \approx \frac{1}{\langle \sigma v(T) \rangle}\frac{d\langle \sigma v(T) \rangle}{dT}\frac{x(1-x) Q_{\text{fus}} g_\alpha m_f N_a^2 \langle \sigma v(T) \rangle}{A_{\text{DT}}^2 c_v V}. \tag{8}$$

Canceling the like terms then produces

$$\alpha(t) \approx \frac{d\langle \sigma v(T) \rangle}{dT}\frac{x(1-x) Q_{\text{fus}} g_\alpha m_f N_a^2}{A_{\text{DT}}^2 c_v V}, \tag{9}$$

which is the equation for the temporal evolution in α as a function of time. By taking the derivative of $\alpha(t)$, the maximum of $\alpha(t)$ is found to occur when the second derivative of the thermal reactivity equals zero. This is demonstrated in Eq. (10):

$$\dot{\alpha}(t) = \frac{d^2\langle \sigma v(T) \rangle}{dT^2}\frac{dT}{dt}\frac{x(1-x) Q_{\text{fus}} g_\alpha m_f N_a^2}{A_{\text{DT}}^2 c_v V}. \tag{10}$$

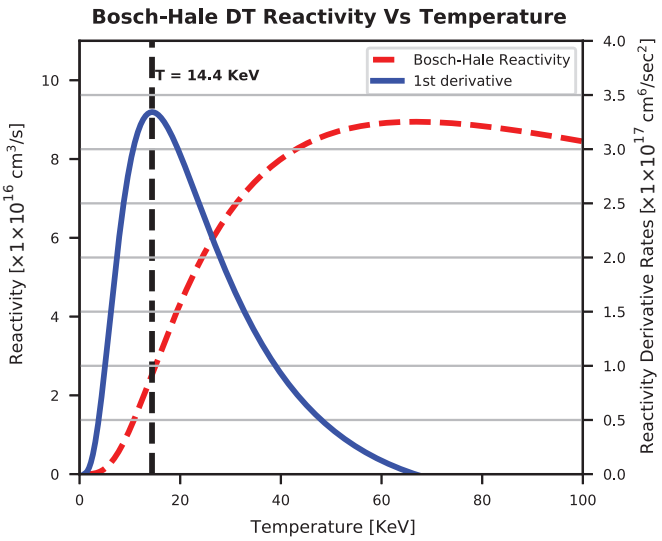

FIG. 2. The Bosch-Hale reactivity fit [40] (dashed red curve) and its first derivative. The dashed black line indicates the location of the maximum of the first derivative.

Therefore, if thermal runaway is achieved, $\dot{\alpha}(t) = 0$ when $\frac{d^2\langle\sigma v(T)\rangle}{dT^2} = 0$ or the first derivative of the reactivity $\frac{d\langle\sigma v(T)\rangle}{dT}$ hits its maximum. This condition is set by the shape of the fusion cross section and will occur at different temperatures for different fusion reactions. This demonstrates that in thermal runaway the α curve will reach its maximum, $\alpha_{\max}$, due to the first derivative of the thermal reactivity.

To investigate where this occurs for DT fusion, the thermal reactivity and its derivatives are plotted in Fig. 2 using the reactivity fit from Bosch and Hale [40], which is considered the most commonly used fit to the DT thermal reactivity. The condition for $\alpha_{\max}$ is met at a temperature of 14.4 keV $\pm$ 10% based on the uncertainty reported in the correlation and the DT cross-section experimental data. Table I shows the condition for other ICF fuels of interest. Since the resonance in the fusion cross section is occurring at much higher energies than the DT reaction, these reactions have much higher temperatures for the occurrence of $\alpha_{\max}$. Since DT is the most applicable fuel for ICF, the rest of the paper will focus specifically on utilizing the DT reaction.

Table I implies that for a DT fusion system where the igniting plasma is able to achieve thermal runaway the temperature at 14.4 keV will cause a fiducial signal in the reaction history where the α curve reaches its maximum and will be a distinct signature of thermal runaway. With the temperature and the energy per fusion reaction known, an equation for the value of

TABLE I. Temperature at which the first derivative of the thermal reactivity is at its maxima, from Ref. [40].

Reaction	Temperature at $\alpha_{\max}$ (keV)	Uncertainty of fit, $\pm$
D(T,n)^{4}He	14.4	1%
D(D,p)T	52.5	1%
D(^{3}He,p)^{4}He	58.8	5%
D(D, n) ^{3}He	58.3	1%

$\alpha_{\max}$ can be found as

$$\alpha_{\max} = \frac{d\langle\sigma v(T_{\alpha_{\max}})\rangle}{dT}\frac{x(1-x)Q_{\text{fus}}g_\alpha\rho N_a^2}{A_{\text{DT}}^2 c_v}, \tag{11}$$

which demonstrates that the temperature at which the value of $\alpha_{\max}$ occurs is at $T_{\alpha_{\max}}$ (14.4 keV for DT fusion), but the magnitude of the value of $\alpha_{\max}$ is a function of the density of the fuel. Typically, the uncertainty in the DT reactivity is reported as $<$10% based on the cross-section measurements [41–43], so this value is known within 1.4 keV.

While this derivation is straightforward, multiple effects can impact the conditions set in Eqs. (10) and (11). For example, the correlation given by Bosch and Hale has been used, but other correlations that fit the R-matrix data for DT fusion exist and have historically been used [44]. Furthermore, it has been assumed that the total energy produced by the fusion reaction is constant. For low-areal-density systems, charged particle transport introduces a dependence on the fraction of the α-particle energy deposited into the fuel mass on both temperature and areal density. The impacts of these effects are explored in Appendixes A and B and yield the equation

$$\alpha_{\max} = \frac{d\langle\sigma v(T_{\alpha_{\max}})\rangle}{dT}\frac{x(1-x)Q_\alpha f_\alpha g_\alpha\rho N_a^2}{A_{\text{DT}}^2 c_v}, \tag{12}$$

where Q_α is the α-particle energy released in a DT fusion reaction and f_α is the fractional value of the α-particle energy deposited in the fuel and is given by

$$f_\alpha = 0.2117\ln(\rho R \times 1000) - 0.6608 \tag{13}$$

from a simplified charged particle transport model (Appendix B).

III. COMPARISON WITH SIMULATION

The analytical formula derived in subsection of Sec. II shows that the timing of $\alpha_{\max}$ will occur during runaway at 14.4 keV. Appendix B shows that charged particle transport itself does not impact the occurrence of the phenomenon but rather modifies the magnitude of $\alpha_{\max}$ and reduces the temperature of its occurrence.

ICF implosions, however, are not static and the dynamics of the implosion phase, which seed the hot-spot ignition and burn propagation, and the expansion phase, where rapid increase in pressure causes the fuel to expand and decrease in density, require radiation hydrodynamics codes to properly model. Comparison with these codes is critical for understanding whether the phenomenon of $\alpha_{\max}$ will occur in a real ICF implosion.

To model the ICF implosion, the Eulerian radiation hydrodynamics code XRAGE [45–47] was used to simulate the NIF Hybrid-E designs which can experimentally achieve ignition. The implosion was driven by a frequency-dependent source (FDS) generated from integrated (capsule and hohlraum) simulations using the HYDRA [48] code. Simulations of the Hybrid-E [49] igniting design were run including a one-dimensional (1D) clean implosion, and then with varying degrees of fusion yield by adding preheat into the ice layer [19,50]. Figure 3 shows example results of the 1D preheat simulations and their respective yields to show the differences in the reaction history and its α curve for a nonigniting

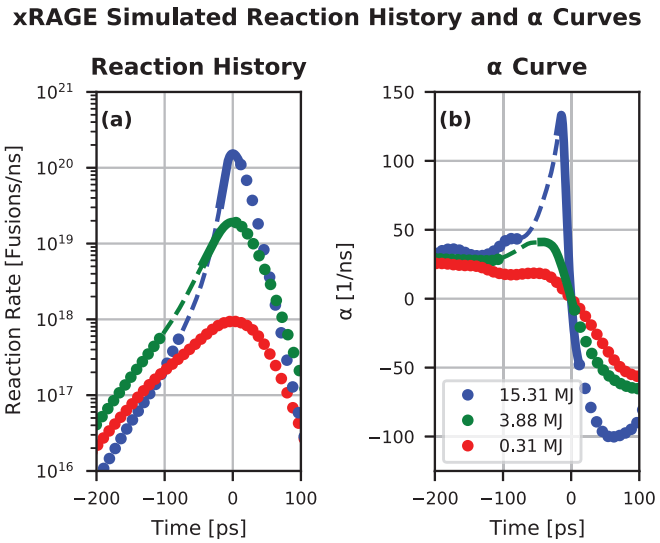

FIG. 3. The XRAGE-simulated reaction history for (a) three selected yield regimes and (b) their respective α curves, corresponding to Fig. 1. The dotted lines denote the compression- and expansion-dominated regions, dashed lines represent the propagating burn phase from mass ablation, and the solid lines represent the region where the temperature changes faster than the areal density in Fig. 1.

plasma, a marginally igniting plasma, and a robustly igniting implosion performance close to the 1D clean yield.

The results in Fig. 4 demonstrate that the robustly igniting implosions (blue and orange curves) generate a strong spike due to the rapid mass increase during the burn-propagation phase as well as a temperature increase, followed by the rapid increase in temperature. This rapid temperature increase occurs after the occurrence of α_{max} and, once the hot-spot temperature reaches the predicted temperature region (shaded grey and red regions), the α curve begins to decrease in magnitude with increasing temperature. In comparison, the marginally igniting implosion, which does not enter the thermal runaway regime (green curve), rolls over and α_{max} is not in the predicted region of the thermal runaway condition. This is due to the rapid expansion of the fuel, which stops the hot spot from entering the thermal runaway regime. These examples are from a limited subset of a larger simulation dataset.

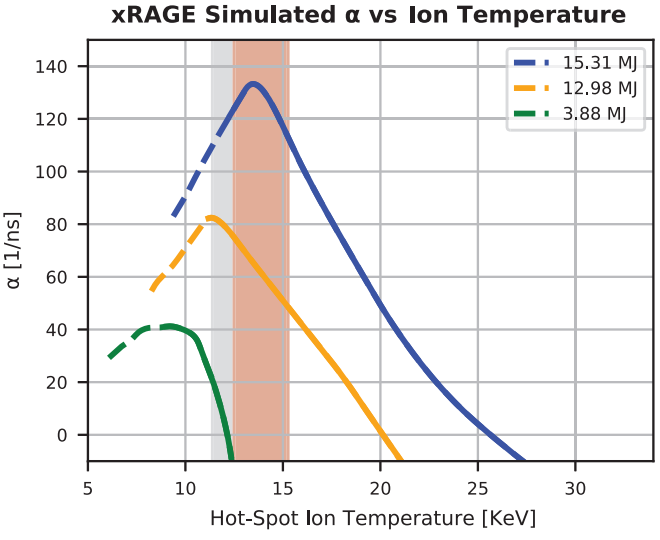

FIG. 4. Simulated α curve as a function of ion temperature. The dashed vs solid regions of the curves indicate the region of propagating burn and thermal runaway, respectively. The shaded red region is the predicted point of α_{max} from theory within the cross-section data. The shaded grey region is the expected region associated with the inherent experimental cross-section uncertainty and accounting for charged particle transport.

This decreasing magnitude of the α curve with respect to temperature in Fig. 4 is easily explained by Eq. (10) and Fig. 2. While Eq. (10) shows that the time derivative of α will increase with the time derivative of temperature, Fig. 2 shows that the first derivative of the thermal reactivity is decreasing in magnitude after 14.4 keV and therefore the second derivative of the reactivity with respect to temperature will be negative. Applying this to Eq. (10) then demonstrates that the time derivative of α will be negative with increasing temperature.

In order to test the sensitivity of the occurrence of α_{max} to the burn degradation mechanism, 200 XRAGE simulations with varying degradation mechanisms in one and two dimensions were run and their values of α_{max} vs yield and temperature were tallied and followed the simulation methodologies in Ref. [19]. These simulations included the 1D degradation mechanisms of preheat, premix, and a dynamic mix model, as well as two-dimensional (2D) degradations such as ablator defects and drive asymmetry. The impact of changing the tungsten dopant in the HDC layer was also assessed; it can either enhance or degrade the yield, depending on the amount of tungsten added to the HDC shell. The simulation yields were normalized to the nominal 1D Hybrid-E point design with a yield of about 20 MJ. These simulations are plotted in Fig. 5 to show that with increasing yield the temperature at α_{max} approaches 14.4 keV and enters the range predicted by experimental uncertainties in the cross-section data and corrections for charged particle transport. Figure 5(b) also shows that magnitude of α_{max} increases as the yield increases.

The temperatures at the occurrence of α_{max} were plotted against the normalized yield over the 1D clean yield to look for the trend in the ion temperature at the occurrence of α_{max} vs the performance of the implosion. The results are shown in Fig. 5(a), which demonstrates that the ion temperature at the occurrence of α_{max} approaches the 14.4-keV value asymptotically and for the robustly burning implosions which seed a thermal runaway. The value is within the anticipated region of the occurrence of the temperature at α_{max} for the charged particle transport model obtained from the simple numerical correlation in Fig. 8. The average value for the simulation study was found to be 12.5 keV $\pm$ 10% for the robustly igniting implosions; 88% of the implosions in the thermal runaway regime were within the presented temperature regime for the correlation of charged particle transport and the DT cross-section uncertainty (grey shaded region). The general trend agrees with the results that isolate charged particle transport in Appendix B.

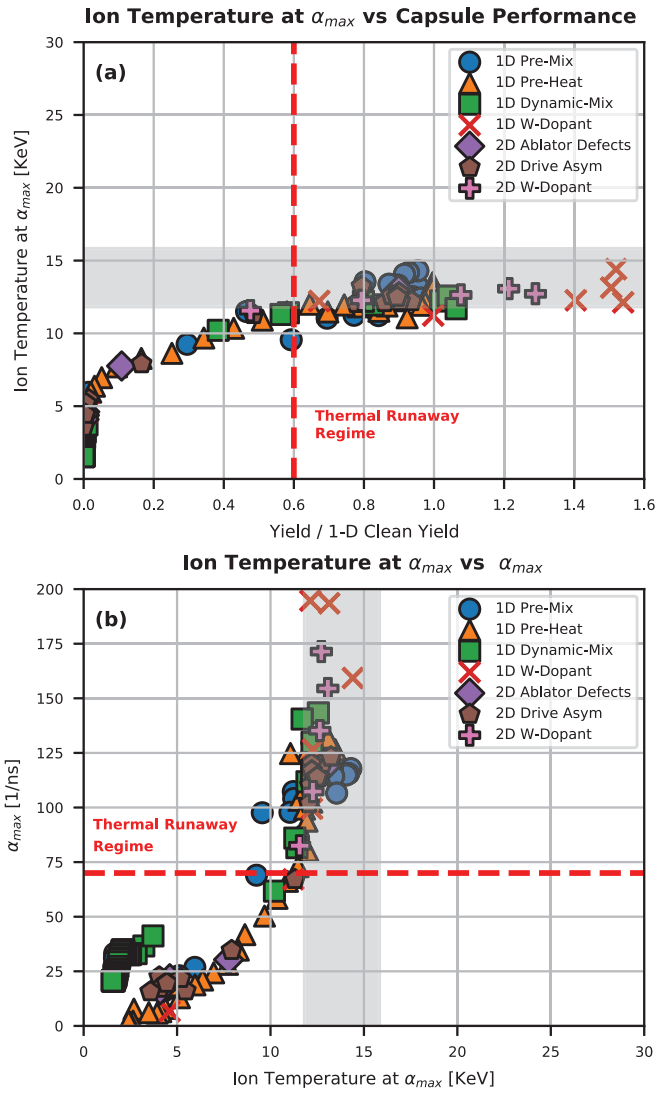

FIG. 5. (a) The XRAGE-predicted ion temperature at $\alpha_{\max}$ as a function of the fraction yield over the 1D clean implosion and (b) the XRAGE-predicted magnitude of $\alpha_{\max}$ at the plotted temperatures. The dashed red line shows the approximate region where thermal runaway begins to occur. The grey region is the temperature expected from a 10% uncertainty due to charged particle transport and the DT cross-section uncertainties.

Figure 5(b) shows the general trend of the magnitude of $\alpha_{\max}$ as a function of the temperature at the occurrence of $\alpha_{\max}$. The dashed red line in Fig. 5(b) corresponds with the dashed line in Fig. 5(a), where the transition into the thermal runaway occurs, which corresponds with a value of $\alpha_{\max} = 70$. Analysis of these data shows that 98% of the implosions within the thermal runaway regime predicted by the simulations have a value of $\alpha_{\max} > 70\ \text{ns}^{-1}$ and 100% have a value of $\alpha_{\max} > 60\ \text{ns}^{-1}$. While the simulations are in general agreement with the trend predicted by theory that the α curve will decrease in magnitude after the temperature of 14.4 keV is reached, the simulations also predict that the value of $\alpha_{\max} > 60$ and the α curve decreasing in magnitude on the rising edge of the reaction history during the deceleration phase of the implosion is indicative of the thermal runaway regime.

IV. DISCUSSION

The occurrence of a maximum in the α curve in an ignited plasma that has seeded a thermal instability demonstrates a unique feature that can be measured when the plasma transitions to the thermal runaway regime. This is due to the change in concavity of the DT fusion thermal reactivity due to the DT fusion resonance-enhanced DT cross section. This can be readily measured with currently available reaction history diagnostics on the NIF, the only facility in the world where igniting plasmas have been produced in a laboratory setting. The database of NIF reaction history is currently being analyzed to investigate if thermal runaway has been measured. The simulation work presented here, however, implies that the NIF implosions are close to where simulations predict this effect (at yields above 8 MJ).

The occurrence of this phenomenon in fusion systems undergoing thermal runaway is supported by theoretical calculations (Sec. II), as well as full 1D and 2D radiation hydrodynamics simulations that capture the full multiphysics processes that occur in an ICF implosion (Sec. III). The occurrence of $\alpha_{\max}$ at a single temperature also provides a fiducial temperature that can be used as a boundary condition to solve Eq. (3) for the time-resolved ion temperature. This would enable true spatially averaged, time-resolved ion temperature to be measured in an ICF implosion for robustly igniting implosions. For the range of yields anticipated on the NIF (2–20 MJ), the current diagnostics have been found to meet the temporal resolution requirements of less than 10 ps [51]. However, in the thermal runaway regime, in order to see the rise of the α curve up to $\alpha_{\max}$ during the burn propagation, a higher dynamic range detector will be needed [52].

While the focus of the paper has been on DT fusion reactions in an ICF experiment, theoretically, there is no reason why this effect should not occur in other fusion schemes such as magneto-inertial fusion (MIF) or any other system that exhibits thermal runaway. This measurement will enable the transition from a marginally igniting implosion, where the thermal instability is tamped by the rapid expansion, to a robustly igniting implosion in ICF, where the thermal instability increases faster than the rapid expansion rate to be measured.

The occurrence of $\alpha_{\max}$ on the rising edge of the reaction history was found to be due to the DT fusion cross-section resonance changing the shape of the thermal reactivity at 14.4 keV during thermal runaway. This impacts the shape of the α curve, causing the "spike" shown in Fig. 3(b) where the rising edge of α increases with temperature and then falls with increasing temperature. The decreasing magnitude of the α curve while the reaction rate is increasing demonstrates that the reaction history curve will be concave down but increasing in magnitude on the rising edge after the 14.4-keV point and the burn width will get smaller. This shows there is an effect that decreases the burn width outside of the increasingly rapid expansion in the ignition regime and explains the change in the scaling of burn width with the transition to the robust ignition regime given in Ref. [19]. This spike might be challenging to measure due to the limited dynamic range

of reaction history diagnostics currently available on the NIF. The results from the simulations in Fig. 5(b) demonstrated that the magnitude of α_{max} trends with yield in the thermal runaway regime, which corresponds to a value of $\alpha_{max} > 60\ ns^{-1}$. This leads to the diagnostic criterion for thermal runaway that the magnitude of α is decreasing on the rising edge of the reaction history measurement and the measured magnitude is $\alpha > 60\ ns^{-1}$, which will imply that the spike occurred even if it is not directly measured. Such a criterion will be used to assess the presence of thermal runaway in upcoming high-yield fusion experiments.

V. CONCLUSIONS

This work demonstrated that to the resonance of the DT fusion cross section, when thermal runaway is seeded in an ICF plasma, there will be a maximum in the logarithmic derivative of the nuclear reaction rate (the "α curve") with a magnitude greater than 70 ns^{-1} at a temperature of 14.4 keV. This was supported by derivation in analytical theory, simple numerical models of a static hot spot, and radiation hydrodynamic simulations. This effect was found to occur at a temperature between 11.6 and 15.6 keV depending on the choice of thermal reactivity function in the literature. For the most commonly used reactivity, it is calculated to occur at 14.4 keV. Numerical models were used to isolate the effect of charged -particle transport and it was found for ignitionrelevant areal densities ($\rho R > 400\ mg/cm^2$) that the impact was less than 12%. Furthermore, the magnitude of α_{max} is also diagnostically relevant, with a decreasing value of α on the rising edge of the burn history with a magnitude of $\alpha_{max} > 70\ ns^{-1}$, which was found to be indicative of thermal runaway. The occurrence of this phenomenon shows that there is a measurable fiducial value in igniting plasmas that can be used to indicate the presence of thermal runaway. This metric is unique in that it measures a specific point in time rather than an average value, and will be used to assess the presence of thermal runaway in ignited plasmas for future, higher-yield implosions.

ACKNOWLEDGMENTS

The authors would like to thank R. Betti at the Laboratory for Laser Energetics and S. Haan at LLNL for their useful discussions, as well as A. Kritcher at LLNL for the use of the FDS from the HYDRA code. This work was performed by the Los Alamos National Laboratory, operated by Triad National Security, LLC, for the National Nuclear Security Administration (NNSA) of the U.S. Department of Energy (DOE) under Contract No. 89233218CNA000001. This material is based upon work supported by the U.S. Department of Energy (National Nuclear Security Administration) University of Rochester "National Inertial Confinement Fusion Program" under Award No. DE-NA0004144.

DATA AVAILABILITY

The data that support the findings of this article are not publicly available upon publication because it is not technically feasible and/or the cost of preparing, depositing, and hosting the data would be prohibitive within the terms of this research project. The data are available from the authors upon reasonable request.

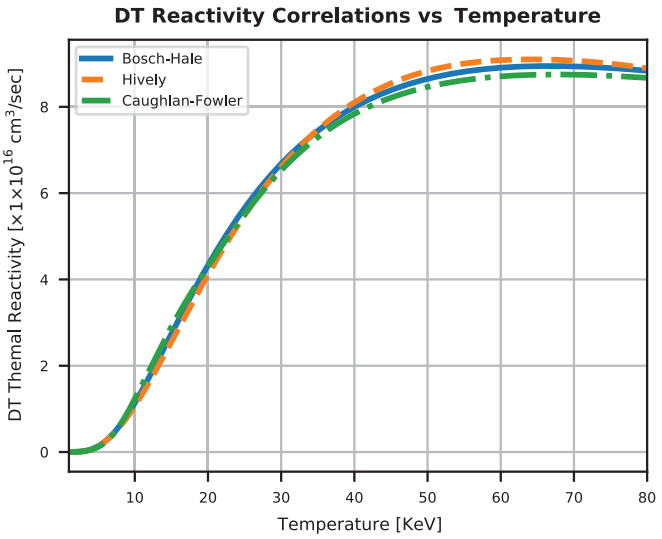

FIG. 6. The Bosch-Hale (solid blue curve), Hively (dashed orange curve), and Caughlan-Fowler (dash-dotted green curve) reactivity correlations.

APPENDIX A: IMPACT OF REACTIVITY FUNCTION

Thus far the condition for α_{max} has utilized the cross-section data from Ref. [40]. While a maximum and minimum for the first derivative are implied by the shape of the resonance of the DT cross section [53], there are other functions used in the literature for the thermal reactivity. The main functions fit to the reactivity, presented by Hively [54] and Coughlan and Fowler [44], all fit *R*-matrix calculations utilizing the DT cross-section measurements. These functions, along with the Bosch-Hale thermal reactivity, are plotted in Fig. 6.

These curves where then differentiated and the maxima of the first derivative of the DT reactivity are given in Table II. The errors of the location of the DT are also shown in the table and use the errors of the fit to the R-Matrix data presented in the respective papers. The average of all three temperatures was found to be 13.88 KeV with an uncertainty of approximately 16% or 2.2 KeV.

These data imply that the occurrence of this effect is not due to the choice in correlation; however, there is some discrepancy in the fits as to at what temperature this effect occurs, especially with the fit given by Coughlan and Fowler.

TABLE II. Temperatures for α_{max} for each of the DT reactivity correlations.

Correlation	Temperature at α_{max} (keV)	Uncertainty (±%)
Bosch-Hale	14.42	1%
Hively	15.64	1%
Coughlan-Fowler	11.57	5%
Average value	13.88	15.6%

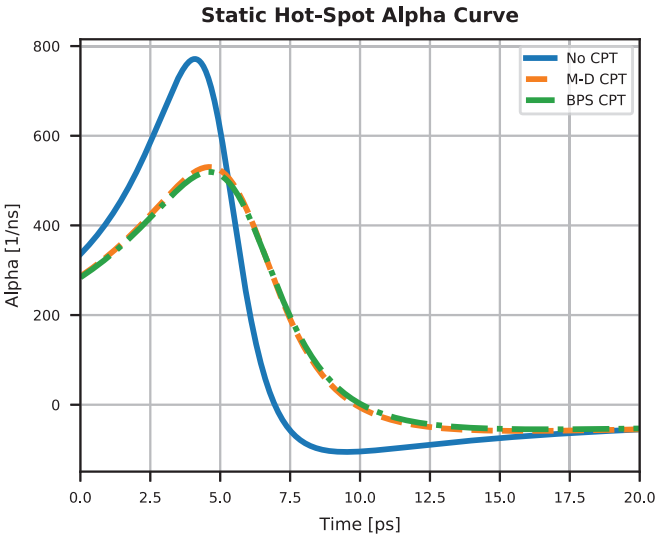

FIG. 7. The baseline solution without charged particle transport (CPT) (solid blue curve), with MD CPT (dashed orange curve), and with BPS CPT (dash-dotted green curve), showing the occurrence of $\alpha_{\max}$ on a chosen CPT model.

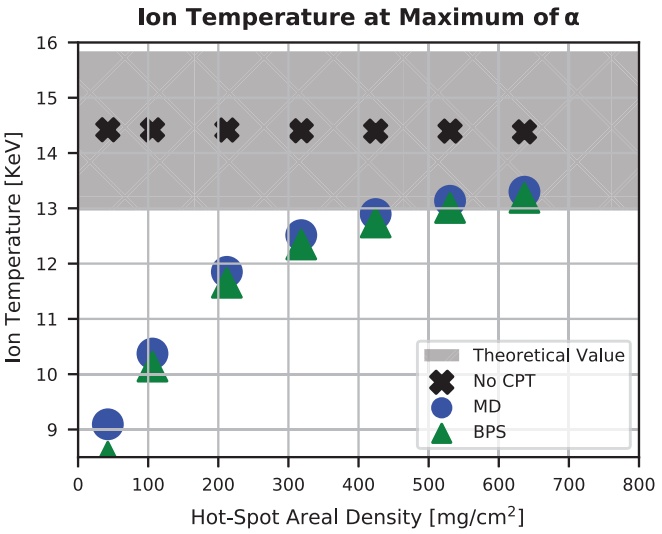

FIG. 8. The value of $T_{\alpha_{\max}}$ as a function of areal density for each of the numerical models demonstrating the effect of CPT on the temperature value. The shaded region is the theoretical prediction including the experimental uncertainties on the DT fusion reactivity.

Understanding at what temperature the inflection point occurs more accurately will require more experimental data to better constrain fits to the DT reactivity in this region. Inertial confinement fusion implosions, and their ability to create a thermal plasma, could be leveraged for such a study to be done.

APPENDIX B: IMPACT OF CHARGED PARTICLE TRANSPORT

The total fusion energy deposited in the fuel, Q_{fus}, will be modified by some fraction of the total energy if the spatial scale is small enough and the density is low enough for both the neutron and α-particle energy for DT fusion [55], and will be of the form

$$Q_{\text{DT}} = f_\alpha Q_\alpha + f_n Q_n,$$

where f_α is the fraction of the α particle, Q_α is the α-particle energy (3.5 MeV), f_n is the fraction of the neutron energy deposited in the fuel, and Q_n is the neutron energy from DT fusion (14.1 MeV). At the low areal densities currently accessible in laboratories, neutron transport is considered negligible in ICF and is typically ignored.

The α-particle stopping power in hot, dense plasmas is difficult to calculate and typically requires numerical simulations. For this work, to estimate the value of f_α the work from Zylstra and Hurricane [56] was used. A simple numerical code using a first-order Euler method which solves the analytical form of the runaway burn equations for a static hot spot is given in subsection of Sec. II with time steps of 1 fs. Figure 7 shows the α curve as a function of time with and without charged particle transport, utilizing a Brown-Preston-Singleton (BPS) model [57] and a Maynard-Deutsch (MD) [58] model. The initial areal density was varied with a starting ignition temperature of 6 keV, which is believed to be representative of NIF hot-spot conditions when α heating takes over.

The example solutions show that the heating rate is decreased and therefore the occurrence of $\alpha_{\max}$ is delayed for the CPT models, but the difference between the two CPT models was negligible. The results of the areal density sweep are shown in Fig. 8. The temperatures at which $\alpha_{\max}$ occur were then plotted in Fig. 8. The figure demonstrates that at low areal densities the stopping power of the α particle has a large impact on the value of $T_{\alpha_{\max}}$, with a 34% reduction at 50 mg/cm^2. At NIF hot-spot relevant areal densities (>400 mg/cm^2), the effect is less than 12% and decreases with increasing areal densities. From the simulations shown in Sec. III, all of the simulations that seed a thermal instability reach areal densities greater than 600 mg/cm^2 due to the rapid rate of ablation of ice mass into the fuel, and the effect is less than 12%.

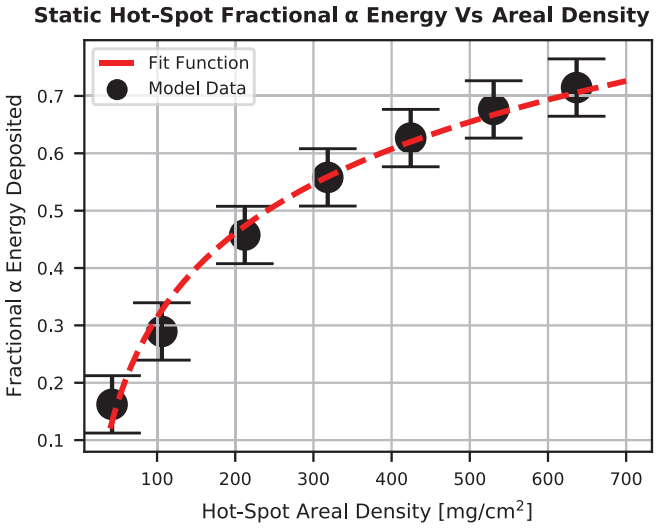

FIG. 9. The value of f_α as a function of areal density from the BPS model.

The impact of the charged-particle transport also shows the magnitude of $\alpha_{\max}$ due to the introduction of the f_α term into Eq. (10). The values of f_α from the numerical model from Figs. 7 and 8 are shown in Fig. 9. A logarithmic curve was fit to the numerical model to use a function of f_α and is given in Eq. (11):

$$f_\alpha = 0.2117 \ln\left(\frac{\rho R}{1000}\right) - 0.6608, \tag{B1}$$

where ρR is in mg/cm^2. This leads to the modified form of Eq. (10),

$$\alpha_{\max} = Q_\alpha f_\alpha \frac{d\langle\sigma v(T_{\alpha_{\max}})\rangle}{dT} g_\alpha \rho \frac{N_a^2}{A^2 c_p}, \tag{B2}$$

with the f_α term introducing a scale length as in Eq. (8) due to the areal density dependence. The impact of neutron heating in the hot spot does not become significant below 1 g/cm^2, which is beyond the range of ICF experiments.

[1] J. Nuckolls, *et al.*, Laser compression of matter to super-high densities: Thermonuclear (CTR) applications, Nature (London). **239**, 139 (1972).

[2] R. C. Kirkpatrick and J. A. Wheeler, The physics of DT ignition in small fusion targets, Nucl. Fusion **21**, 389 (1981).

[3] S. Atzeni and J. Meyer-ter-Vehn, *The Physics of Inertial Fusion* (Oxford University Press, Oxford, UK, 2009).

[4] M. D. Rosen, The physics issues that determine inertial confinement fusion target gain and driver requirements: A tutorial, Phys. Plasmas **6**, 1690 (1999).

[5] J. Lindl, Development of the indirect-drive approach to inertial confinement fusion and the target physics basis for ignition and gain, Phys. Plasmas **2**, 3933 (1995).

[6] J. D. Lindl, *et al.*, The physics basis for ignition using indirect-drive targets on the National Ignition Facility, Phys. Plasmas **11**, 339 (2004).

[7] N. B. Meezan, *et al.*, National Ignition Campaign hohlraum energetics, Phys. Plasmas **17**, 056304 (2010).

[8] D. C. Wilson, *et al.*, Single and double shell ignition targets for the national ignition facility at 527 nm, Phys. Plasmas **28**, 052704 (2021).

[9] O. A. Hurricane, *et al.*, Inertially confined fusion plasmas dominated by alpha-particle self-heating, Nat. Phys. **12**, 800 (2016).

[10] A. B. Zylstra, *et al.*, Burning plasma achieved in inertial fusion, Nature (London) **601**, 542 (2022).

[11] H. Abu-Shawareb, *et al.* (Indirect Drive ICF Collaboration), Achievement of target gain larger than unity in an inertial fusion experiment, Phys. Rev. Lett. **132**, 065102 (2024).

[12] W. Daughton, *et al.*, Influence of mass ablation on ignition and burn propagation in layered fusion capsules, Phys. Plasmas **30**, 012704 (2023).

[13] A. R. Christopherson, R. Betti, and J. D. Lindl, Thermonuclear ignition and the onset of propagating burn in inertial fusion implosions, Phys. Rev. E **99**, 021201(R) (2019).

[14] R. Betti, *et al.*, Hot-spot dynamics and deceleration-phase Rayleigh-Taylor instability of imploding inertial confinement fusion capsules, Phys. Plasmas **8**, 5257 (2001).

[15] Y. Saillard, Acceleration and deceleration model of indirect drive ICF capsules, Nucl. Fusion **46**, 1017 (2006).

[16] J. Garnier and C. Cherfils, A multiscale analysis of the hotspot dynamics during the deceleration phase of inertial confinement capsules, Phys. Plasmas **12**, 012704 (2004).

[17] J. Sanz, *et al.*, Self-consistent analysis of the hot spot dynamics for inertial confinement fusion capsules, Phys. Plasmas **12**, 112702 (2005).

[18] A. Campos, Multi-physics simulations of ICF capsules using high-order finite-element discretizations, in *66th Annual Meeting of the APS Division of Plasma Physics* (Bulletin of the American Physical Society, Atlanta, 2024).

[19] B. M. Haines, *et al.*, Simulated signatures of ignition, Phys. Plasmas **31**, 042705 (2024).

[20] T. J. Murphy, *et al.*, Ion-temperature measurement of indirectly driven implosions using a geometry-compensated neutron time-of-flight detector, Rev. Sci. Instrum. **66**, 930 (1995).

[21] M. G. Johnson, *et al.*, Neutron spectrometry—An essential tool for diagnosing implosions at the National Ignition Facility, Rev. Sci. Instrum. **83**, 10D308 (2012).

[22] D. H. Munro, Interpreting inertial fusion neutron spectra, Nucl. Fusion **56**, 036001 (2016).

[23] D. J. Schlossberg, *et al.*, Observation of hydrodynamic flows in imploding fusion plasmas on the national ignition facility, Phys. Rev. Lett. **127**, 125001 (2021).

[24] S. Haan, *Time-Dependent Neutron Spectrum Features from hydra Simulations* (Lawrence Livermore National Laboratory, Los Alamos, NM, 2024).

[25] D. C. Wilson, *et al.*, Diagnosing ignition with DT reaction history, Rev. Sci. Instrum. **79**, 10E525 (2008).

[26] Y. Kim and H. W. Herrmann, Gamma-ray measurements for inertial confinement fusion applications, Rev. Sci. Instrum. **94**, 041101 (2023).

[27] J. A. Frenje, Nuclear diagnostics for inertial confinement fusion (ICF) plasmas, Plasma Phys. Controlled Fusion **62**, 023001 (2020).

[28] Y. Kim, *et al.*, Measurements of fusion reaction history in inertially confined burning plasmas, Phys. Plasmas **30**, 072706 (2023).

[29] O. A. Hurricane, *et al.*, Energy principles of scientific breakeven in an inertial fusion experiment, Phys. Rev. Lett. **132**, 065103 (2024).

[30] O. A. Hurricane, *et al.*, Beyond alpha-heating: Driving inertially confined fusion implosions toward a burning-plasma state on the National Ignition Facility, Plasma Phys. Controlled Fusion **61**, 014033 (2019).

[31] O. A. Hurricane, *et al.*, An analytic asymmetric-piston model for the impact of mode-1 shell asymmetry on ICF implosions, Phys. Plasmas **27**, 062704 (2020).

[32] J. L. Tuck, Thermonuclear reaction rates, Nucl. Fusion **1**, 201 (1961).

[33] H. A. Bethe, Energy production in stars, Phys. Rev. **55**, 434 (1939).

[34] K. D. Meaney, *et al.*, Simple analytic fusion hot spot models for fusion reaction history, Phys. Plasmas **32**, 122703 (2025).

[35] H. Geppert-Kleinrath, *et al.*, Pulse dilation gas Cherenkov detector for ultra-fast gamma reaction history at the NIF (invited), Rev. Sci. Instrum. **89**, 10I146 (2018).
[36] H. Geppert-Kleinrath, *et al.*, Commissioning the new pulse dilation gas Cherenkov detector at the National Ignition Facility, High Energy Density Phys. **37**, 100862 (2020).
[37] J. R. Langenbrunner and J. M. Booker, Chain rule approach for calculating the time-derivative of flux (2017), doi: 10.2172/1398942.
[38] A. R. Christopherson, *et al.*, A comprehensive alpha-heating model for inertial confinement fusion, Phys. Plasmas **25**, 012703 (2018).
[39] R. Betti, *et al.*, Alpha heating and burning plasmas in inertial confinement fusion, J. Phys. Conf. Ser. **717**, 012007 (2016).
[40] H. S. Bosch and G. M. Hale, Improved formulas for fusion cross-sections and thermal reactivities, Nucl. Fusion **32**, 611 (1992).
[41] R. T. Santoro and J. Barish, *Cross-Section Sensitivity of the D-T Fusion Probability and the D-T and T-T Reaction Rates* (Oak Ridge National Laboratory, Oak Ridge, TN, 1975).
[42] N. Otuka, *et al.*, Towards a more complete and accurate experimental nuclear reaction data library (EXFOR): International collaboration between nuclear reaction data centres (NRDC), Nucl. Data Sheets **120**, 272 (2014).
[43] M. B. Chadwick, *et al.*, ENDF/B-VII.1 nuclear data for science and technology: Cross sections, covariances, fission product yields and decay data, Nucl. Data Sheets **112**, 2887 (2011).
[44] G. R. Caughlan and W. A. Fowler, Thermonuclear reaction rates V, At. Data Nucl. Data Tables **40**, 283 (1988).
[45] M. Gittings, *et al.*, The RAGE radiation-hydrodynamic code, Comput. Sci. Discovery **1**, 015005 (2008).
[46] B. M. Haines, *et al.*, Coupling laser physics to radiation-hydrodynamics, Comput. Fluids **201**, 104478 (2020).
[47] B. M. Haines, *et al.*, High-resolution modeling of indirectly driven high-convergence layered inertial confinement fusion capsule implosions, Phys. Plasmas **24**, 052701 (2017).
[48] S. H. Langer, I. Karlin, and M. M. Marinak, Performance characteristics of HYDRA - a multi-physics simulation code from Lawrence Livermore National Laboratory (2014), doi:10.2172/1116974.
[49] A. L. Kritcher, *et al.*, Design of the first fusion experiment to achieve target energy gain $G > 1$, Phys. Rev. E **109**, 025204 (2024).
[50] B. M. Haines, *et al.*, A mechanism for reduced compression in indirectly driven layered capsule implosions, Phys. Plasmas **29**, 042704 (2022).
[51] W. M. Wood, Reaction history measurement requirements, Report No. LA-UR-06-6891 (Los Alamos National Laboratory, 1991).
[52] J. M. Mack, *et al.*, Multiplexed gas Cherenkov detector for reaction-history measurements, Rev. Sci. Instrum. **77**, 10E728 (2006).
[53] M. B. Chadwick, *et al.*, Early nuclear fusion cross-section advances 1934–1952 and comparison to today's ENDF data, Fusion Sci. Technol. **80**, S9 (2024).
[54] L. M. Hively, A simple computational form for Maxwellian reactivities, Nucl. Technol. Fusion **3**, 199 (1983).
[55] J. R. L. Singleton, Charged particle stopping power effects on ignition: Some results from an exact calculation, Phys. Plasmas **15**, 056302 (2008).
[56] A. B. Zylstra and O. A. Hurricane, On alpha-particle transport in inertial fusion, Phys. Plasmas **26**, 062701 (2019).
[57] L. S. Brown, D. L. Preston, and R. L. Singleton, Jr., Charged particle motion in a highly ionized plasma, Phys. Rep. **410**, 237 (2005).
[58] G. Maynard and C. Deutsch, Born random phase approximation for ion stopping in an arbitrarily degenerate electron fluid, J. Phys. France **46**, 1113 (1985).